Journal of
Marine Science and Engineering

MDPI

Article

On the Sediment Dynamics in a Tidally Energetic Channel: The Inner Sound, Northern Scotland

Jason McIlvenny [1,*], Duncan Tamsett [1,2], Philip Gillibrand [1] and Lonneke Goddijn-Murphy [1]

[1] Centre for Energy and the Environment, Environmental Research Institute, North Highland College UHI, Ormlie Road, Thurso KW14 7EE, UK; duncan.tamsett@uhi.ac.uk (D.T.); philip.gillibrand@uhi.ac.uk (P.G.); lonneke.goddijn-murphy@uhi.ac.uk (L.G.-M.)

[2] Kongsberg Maritime, Underwater Mapping, Shuttleworth Close, Great Yarmouth, Norfolk NR31 0NQ, UK

* Correspondence: jason.mcilvenny@uhi.ac.uk; Tel.: +44-(0)1847-889-663

Academic Editor: Jens Martin Hovem
Received: 31 December 2015; Accepted: 30 March 2016; Published: 8 April 2016

Abstract: Sediment banks within a fast-flowing tidal channel, the Inner Sound in the Pentland Firth, were mapped using multi-frequency side-scan sonar. This novel technique provides a new tool for seabed sediment and benthic habitat mapping. The sonar data are supplemented by sediment grab and ROV videos. The combined data provide detailed maps of persistent sand and shell banks present in the Sound despite the high energy environment. Acoustic Doppler Current Profiler (ADCP) data and numerical model predictions were used to understand the hydrodynamics of the system. By combining the hydrodynamics and sediment distribution data, we explain the sediment dynamics in the area. Sediment particle shape and density, coupled with persistent features of the hydrodynamics, are the key factors in the distribution of sediment within the channel. Implications for tidal energy development planned for the Sound are discussed.

Keywords: sediment transport; hydrodynamics; settling rates; tidal energy; Pentland Firth

1. Introduction

Over the past decade, the strong tidal flows of the Pentland Firth have been a focus of attention for tidal energy developers, with a number of sites identified and leases granted for tidal energy extraction using tidal turbines. Tidal energy potential for the whole Firth has been estimated to be in the range of 1–18 GW [1], though Adcock *et al.* [2], suggest that a more realistic figure for the maximum available power is 1.9 GW. At the time of writing, the Meygen tidal turbine array, planned for the Inner Sound channel in the Firth (Figure 1), is likely to be the first commercial tidal energy array to be installed anywhere in the world. Tidal current speeds in the Inner Sound have been recorded up to 6 $m \cdot s^{-1}$ during flood spring tides, offering an energy resource of up to 398 MW to the Meygen project [3]. Government consent to deploy tidal turbines and marine energy generation devices in general, is subject to environmental impact assessment, demonstrating little or acceptable environmental effect. These assessments typically focus on collision risk for marine mammals and seabirds, which present the highest impact risks. However, other, more subtle, environmental impacts arising from the deployment of large numbers of tidal turbines can be envisaged. These have been outlined by a number of authors, with the focus being mainly on ecological and socio-economic impacts (e.g., [4,5]).

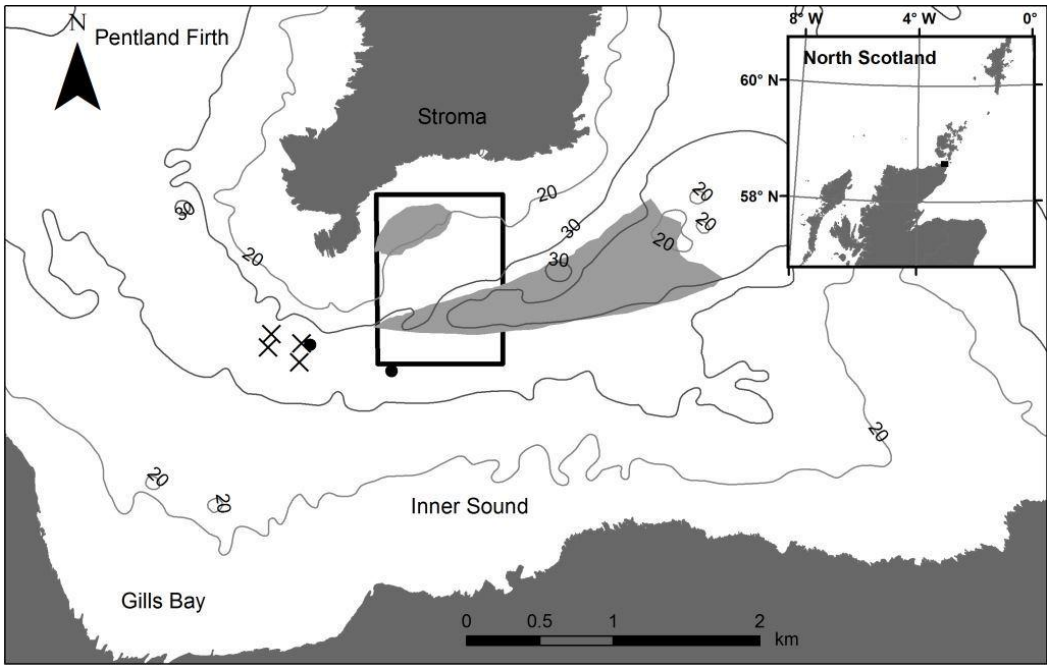

Figure 1. Study site location. The Inner Sound lies between the island of Stroma and Gills Bay on the Scottish mainland. The Pentland Firth lies between the mainland and the Orkney Islands. Also shown; nearshore bathymetry (contours) and the locations of the sediment banks obtained from multi-beam data [3], and ADCP data (●) referred to in Tables 2 and 3 (ADCP 1 is furthest west and ADCP 2 to the east). The positions of the first tidal turbines are noted (x).

To date, one of the potential impacts of tidal energy that has received less attention is sediment transport and the effect of energy extraction on the movement of sediment through these tidally energetic channels. An early study by Neill *et al.* [6], demonstrated that installations of tidal energy convertors in the Bristol Channel had the potential to influence large scale sediment dynamics and bed level changes, and that these impacts were most pronounced in regions where tidal asymmetry was stronger. In a further study, Neill *et al.* [7], found that tidal turbines could also impact sand bank formation and evolution near headlands. In the Pentland Firth, Martin-Short *et al.* [8], used a high resolution hydrodynamic model to identify areas of sediment erosion and deposition, based on critical bed shear stress distributions calculated by the model. They found that installing arrays of more than 85 tidal turbines in the Inner Sound had the potential to significantly displace areas of sediment accumulation from the sides towards the centre of the channel, as the flow was diverted around the array. With still larger arrays of more than 240 turbines, beds of larger sized sediments, such as fine gravel and coarse sand, were also predicted to migrate towards the channel centre. A further study, by Fairley *et al.* [9], extended the modelled sediment transport in the Pentland Firth into predictions of bed level changes, and again investigated the possible effects of turbines deployed in the Inner Sound on sediment deposition and erosion. Changes to sediment deposition and erosion patterns are likely to have knock-on effects on benthic communities that rely on suspended organic material. Harendza [10] found that bed shear stress was closely associated to the composition and distribution of benthic assemblages in the Inner Sound, and developed site-specific habitat suitability models based on physical characteristics both in the absence and presence of tidal turbines.

Martin-Short *et al.* [8], and Fairley *et al.* [9], both noted that accurate sediment modelling is inhibited by a lack of detailed knowledge of local sediment deposits and transport in the area. Fairley *et al.* combined a variety of data to construct a map of sediment type through the Pentland Firth and surrounding area, but detail in the Inner Sound was limited. Sediment banks are known to lie to the west and south of the island of Stroma and in the surrounding region some of which are

composed of carbonate shell [11–14], but the local sediment dynamics, and the potential impacts of tidal energy extraction on the deposits, remains uncertain.

Understanding of the tidal flow through the Pentland Firth has advanced in recent years, due in part to the proliferation of hydrodynamic models (e.g., [1,2,8,9,15] *etc.*) and observational studies (e.g., [16]). Many of the numerical models utilised used unstructured grids, which allow spatial resolution in the model to be concentrated in the area of interest while allowing open boundaries to be located far away. The strong flows through the Firth are generated from the hydraulic pressure head that forms across the channel due to the restriction on the propagation of the tide [15], and in order to capture the forcing of the flow through the Firth it is necessary to accurately simulate the regional tidal regime. Most of the above studies have focussed on the flow through the entire Pentland Firth, without focussing specifically on the Inner Sound.

In this paper, we provide more detailed information on sediment deposits in the Inner Sound to the south of Stroma, where the first tidal turbine array is about to be deployed, and, by analysing measurements and numerical model simulations of local velocity fields, we infer the local sediment dynamics. Firstly, we describe the planar positions of two hydraulically separated sediments with respect to the prevailing tidal flow, based on observations by a new multi-frequency side-scan sonar technique [17]. The side-scan sonar observations are supplemented by video images from a remotely-operated vehicle (ROV) and multi-beam sonar data. The hydrodynamics of the Inner Sound are described from a combination of observations from an underway Acoustic Doppler Current Profiler (ADCP) survey and numerical hydrodynamic modelling. We then speculate that sediment grain size and shape are primarily responsible for the patterns of sedimentation observed with hydraulic behaviour of shell fragments differing from that of mineral sediment [18,19]. Shell and sand respond differently to similar hydrodynamic conditions and belong to two different hydraulic populations [20]. Finally, we use the observed and modelled patterns of current velocity to explain the observed sediment distributions, and speculate on the potential impacts of a large tidal turbine array on those distributions. Bedform classifications used in the paper are based on the classification scheme recommended by the SEPM bedforms and bedding structures research symposium [21].

2. Methods

2.1. Study Site

Our study site is the Inner Sound between the Island of Stroma and the north coast mainland of Scotland (Figure 1). This channel forms the southern arm of the Pentland Firth, which lies between the Orkney Islands and the Scottish mainland and connects the North Sea to the North Atlantic. Water depths in the Inner Sound reach 40 m in the central channel. Shields *et al.* [4] described the Pentland Firth as comprising predominantly of exposed bedrock, but localised sediment deposits are known to exist around Stroma. We conducted acoustic surveys using side-scan sonar, including a novel prototype tri-frequency ("colour") digital sonar, in a focused area within the sound to map the sediment banks to the south of Stroma. The acoustic data were ground-truthed using sediment grab and a remotely-operated-vehicle (ROV) data from earlier surveys.

The survey area was approximately 900 by 1200 m in size. Depths within the study area ranged between 10 and 39 m, with a mean depth of 28 m (depth derived from multi-beam bathymetry [3]), with mostly gentle sloping topography and a tidal range of approximately four metres. The site has been surveyed in the past by a variety of instruments including multi-beam sonar, ADCP, ROV and side-scan sonar.

2.2. Remotely Operated Vehicle

Data were acquired using a small 6.9 m catamaran coastal research vessel "Aurora". Sediment grabs and ROV work were undertaken from the vessel. A small ROV was used (Outland Technologies ROV 1000) which was easily launched from the side of the vessel. A small stills camera was added to

the ROV and two green lasers to give spatial scale to the still images. Sediment grabs were undertaken by hand using a small Van Veen grab. Sediment particle size analysis was undertaken using a standard sieve stack and using the Folk and Ward method for sorting categories [22]. Positions of ROV snapshots and grab samples used in this paper are shown in Figure 2. Not all grabs were successful with only grabs occurring over the two sediment banks successful in recovering a sample.

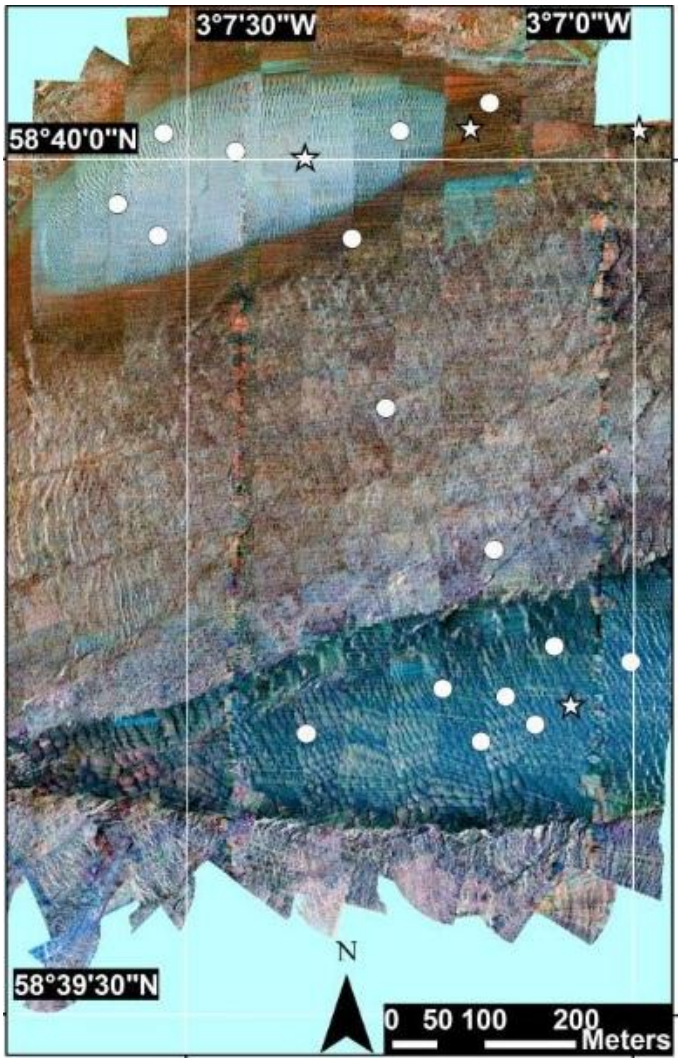

Figure 2. Positions of grab samples (**circles**) and positions of remotely-operated-vehicle (ROV) snapshots (**stars**).

2.3. Side-Scan Sonar

A prototype multi-frequency side-scan sonar system developed by Kongsberg GeoAcoustics Ltd. (Great Yarmouth, UK) [17], was pole mounted to "Aurora" approximately 1 m below the hull. The sonar pings at three frequencies 114, 256, and 410 kHz. The sonar is a basic range-only system and provides no bathymetric data along the trace. The Kongsberg GeoAcoustics Ltd. (Great Yarmouth, UK) propriety software "GeoTexture" was used to process the sonar data. GPS navigation and heading data were provided by a Hemisphere Vector V110 unit mounted directly above the side scan pole mount.

The sonar acoustic data acquired at three ping frequencies constitutes acoustic colour data. These were mapped onto the optical primary colours in the electromagnetic spectrum for human visualisation. Acoustic colour sonar is not a new idea, but it has proved difficult to implement. The sonar backscatter response of the seabed is a function not only of sonar system carrier wave frequency but also of

geometrical spreading and absorption (range); the angular shape of sonar beam functions and seabed backscatter functions; and sonar vehicle roll and seabed slope. Satisfactory estimates of the sonar beam function are the key to successfully applying the angular based corrections. A method to extract sonar beam functions from data affected by sonar vehicle roll is described by Tamsett and Hogarth [23] and this has provided good estimates of sonar beam functions. Correcting for the non-seabed effects on sonar amplitude outlined above, and normalising the seabed response for all angles to that at a reference inclination angle (30°), means that acoustic colour becomes a meaningful property of the seabed. A colour image contains dimensions of information absent in a greyscale image, and is therefore a richer source of information on the nature of the seabed than a greyscale image.

For the purpose of human visualisation, data at sonar frequencies are mapped to optical primary colour frequencies such that the colours red, green, and blue are seen in proportion to the amplitudes of the low-, mid- and high-frequency sonar data respectively. Also, optical colour is generated in such a way that shadow appears white and saturation black; and weakly backscattering seabed as light shades of colour, and strongly backscattering seabed as dark shades of colour using the negative CMY colour scheme the details of which are presented elsewhere [17]. Side-scan sonar swaths were plotted on charts (mosaicked) and overlaid to generate a chart with ensonification (predominantly) to the West, and then underlain for an image for ensonification to the East. Data were frequency equalised over an image used as a standard such that the mean seabed colour response over the whole image is an appropriate mid-shade of grey.

Two side-scan surveys were undertaken in the summer of 2015, survey 1 (May 2015) and survey 2 (June 2015). Survey 1 was undertaken during flood spring tide conditions and survey 2 undertaken during ebb spring tides. The trace length was 120 ms (a maximum range and half-swath width of approximately 90 m). Both surveys were conducted along 15 lines running approximately North-South spaced at 50 m intervals. The area of seabed survey was in each case approximately 900 (N-S) by 1100 (E-W) metres. The time spent at sea was approximately 4 h, plus a similar amount of time to mobilise and demobilise the vessel.

2.4. Acoustic Doppler Current Profiler (ADCP)

Underway ADCP surveys, described by [16], were performed using a 300 kHz Teledyne Workhorse Sentinel ADCP pole-mounted to the research vessel "Aurora" at approximately 1 m below the waterline, and measured vertical profiles of current speed and direction. Beam 3 was rotated 45° away from the vessels centreline. Vessel speed was approximately 6 knots when undertaking the survey. A blanking distance of 2 m was applied and 12 depth bins, each of 2 m thickness, selected. The ADCP operated at 2 Hz with single-ping bottom tracking enabled. The ADCP data were merged with GPS data from an on-board Raymarine GPS system and averaged into ensembles of 15 s. Results from a flood tide survey on 15th April 2009 and an ebb tide survey on 7th April 2009 are reported here. For more details of the survey technique and data processing methodology, refer to [16].

Subsequent to the underway surveys, two 300 kHz upward-looking Teledyne Workhorse ADCPs were deployed in the Inner Sound during February–March 2013. Both instruments were deployed in about 35 m of water to the south of the island of Stroma (Figure 1). The western instrument is denoted "ADCP 1", the eastern instrument "ADCP 2". The ADCPs sampled at 2 Hz, with data subsequently averaged into 1-min ensembles. Bin size was 2 m. Valid data extended from approximately 6.5–30.5 m above the seabed, but have been averaged here into depth-averaged values. Tidal analysis on the depth-averaged data was performed using the T-TIDE software [24].

2.5. Sea Surface Height Data

Sea surface height (SSH) data were collected at Scrabster and John O'Groats using an Aanderaa WLTS 3791A instrument, set to record at 10 min intervals. Nominal instrument accuracy is 0.02 m. SSH data at Stroma were collected using a Valeport TideMaster (accuracy 0.01 m), again with a sampling interval of 10 min. Data from the Inner Sound were obtained from a pressure sensor on the ADCP

(see previous section) with 10 min sampling frequency. Sea level at Wick is routinely measured for the UK National Tide Gauge Network, part of the National Tidal and Sea Level Facility; the hourly data used here from February–March 2013 were obtained from the British Oceanographic Data Centre.

2.6. Hydrodynamic Model

The numerical model RiCOM (River and Coastal Ocean Model) is a general-purpose hydrodynamics and transport model, which solves the standard Reynolds-averaged Navier-Stokes equation (RANS) and the incompressibility condition, applying the hydrostatic and Boussinesq approximations. It has been tested on a variety of benchmarks against both analytical and experimental data sets (e.g., [25–27]). The model has been previously used to investigate the inundation risk from tsunamis and storm surge on the New Zealand coastline [26,28,29], and to study tidal currents in high energy environments [30–32]. Here the model was used to study the highly energetic flow through the Pentland Firth.

The model grid covered the northern Scottish continental shelf. An unstructured mesh was used, with grid resolution increasing from 20 km at the outer boundaries of the model to ~40 m in the Inner Sound. The model was forced at the outer boundaries by seven tidal constituents (O1, K1, Q1, M2, S2, N2, M4) which were taken from the Oregon State University global tide model [33]. No wind forcing was applied and water density was assumed to be constant. Bathymetry was obtained from a variety of sources, amalgamating sources of increasing resolution closer to the coast. The model was run in depth-averaged mode and was used to simulate the flow through the Pentland Firth over the period 18 February–24 March 2013.

Results were calibrated against the sea surface height data from Scrabster, Wick, Stroma, John O'Groats, and the Inner Sound (as described above). Velocity predictions from the model were evaluated against the two simultaneous deployments of ADCPs in the Inner Sound during 2013. More extensive evaluation of the model over the wider domain is ongoing.

Depth-averaged velocity fields were saved every hour. The maximum velocity that occurred at each grid point over the duration of the simulation was also stored. From these maximum velocity fields, a maximum bed stress was calculated [34].

$$\tau_b = \rho C_D U^2 \quad (1)$$

where ρ = 1025 kg·m^{-3} is the water density, C_D = 0.0025 is a drag coefficient and U is the depth-averaged velocity (m·s^{-1}). We use the value of C_D = 0.0025 only for the post-simulation calculation of the maximum bed stress; during the model calibration process, the frictional drag coefficient is tuned to provide the best fit to observations of sea level and velocity.

3. Results

3.1. Side-Scan Sonar

Individual frequency channels reveal different details of the seabed (Figure 3). From the merged colour mosaic image, Figure 3iv; clear distinctions can be made between material types. Merging the three frequencies for colour imaging improves classification results in both supervised and unsupervised classification. Figure 3 shows the results of supervised classification using the same sample training areas to undertake both classifications on the colour composite image, Figure 3v and single frequencies of which the 114 kHz is shown in Figure 3vi.

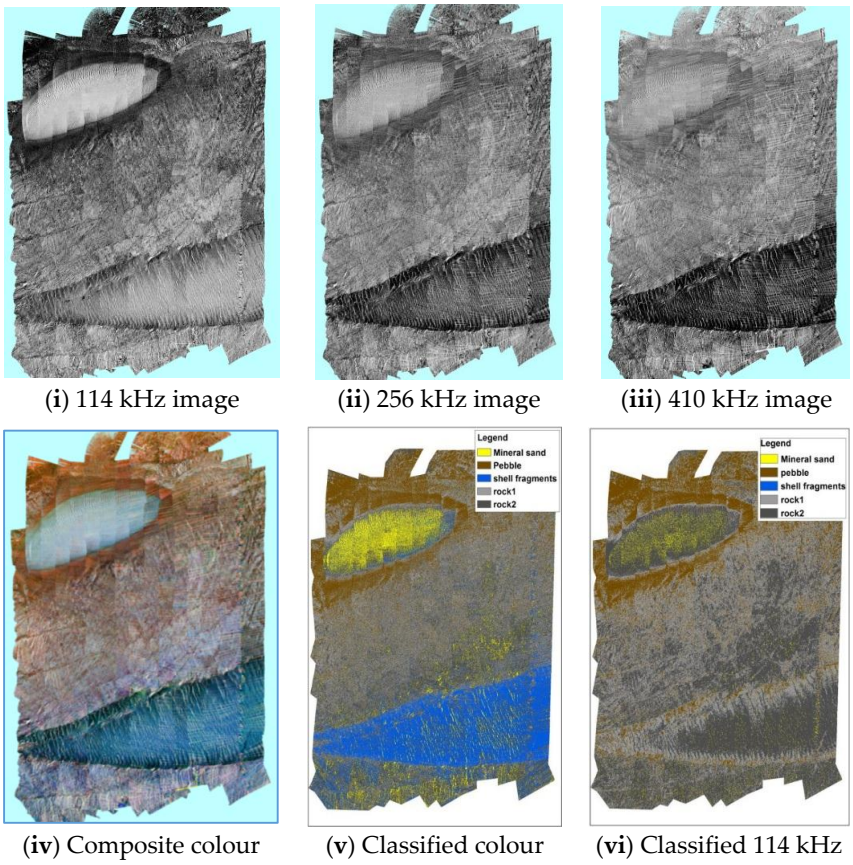

Figure 3. Figures respectively showing the frequency channels of (**i**) 114; (**ii**) 256 and (**iii**) 410 kHz of the study area for survey 1; Images represent an area of approximately 900 by 1130 m. The colour mosaic is shown (**iv**); (**v**) Supervised classification of the composite colour image; (**vi**) Supervised classification of the 114 kHz image.

Two distinct sediment beds are present in the study area and exhibit different acoustic properties. An oval shaped sediment bank is present in the north of the survey area and a wedge shaped sediment bank in the southern part of the survey area. Bedrock in the survey area is Devonian sedimentary rock throughout. Differing acoustic backscattering characteristics from varying amounts of marine growth result in the differing acoustic responses of the bedrock, with colours from reddish brown (heavy coverage) to violet (bare rock) seen in the colour mosaic (Figures 2 and 3). Evidence for several well defined faults can also be detected. A halo of material is seen surrounding the oval bank; the texture and colouring of the material in the processed side-scan image indicates a different material than the surrounding bedrock or material composing the oval shaped northern bank.

The oval shaped sediment bank has a major axis at approximately 70° N. It is approximately 475 m in length along the major axis and 175 m in length along the minor axis. The colour composite image from survey 1 (flood tide survey, June 2016) shows superimposed medium sized subaqueous dunes present on the surface of the oval sediment bank in the north of the bank and small sized subaqueous dunes in the south and centre. The dunes on the northern edge have wavelengths between 5 and 7 m and slope to the west, indicating a westerly current direction. On the southern edge the wavelength is smaller, approximately 2–3 m and slope to the east. In the centre of the sediment bank dune wavelengths are smaller with wavelengths of 1–2 m. The counter-clockwise orientation of the dunes around the bank indicate a circular current or eddy present rotating in a counter-clockwise direction during this survey (flood tide).

The second side-scan survey was undertaken during spring ebb tides. Comparison between the two surveys shows little change in the sediment banks' plan shape or position (Figure 4). The plan

length curvature of some dunes on the northern edge of the oval shaped sand bank show a curve to the west or c shaped plan during survey 1 (flood tide) and show a similar pattern in survey 2 (ebb tide, Figure 4).

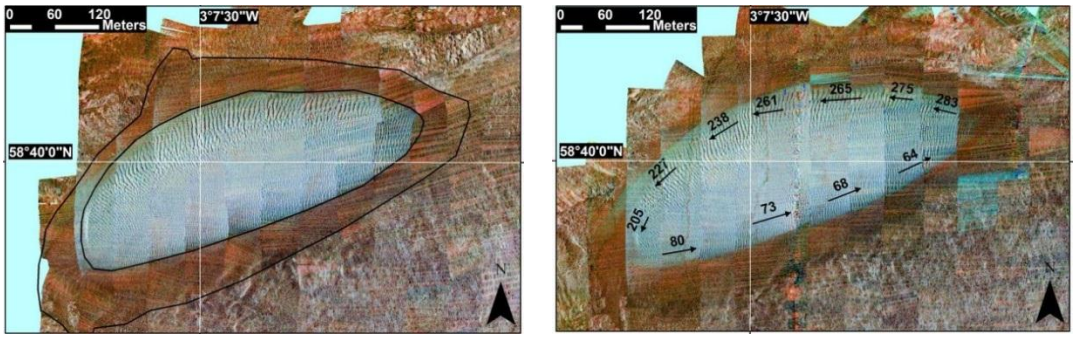

(**i**) (**ii**)

Figure 4. Dune crest directions on the oval shaped sand bank during spring flood tide, June 2015 (**i**) and ebb tide, May 2015 (**ii**). Little change in dune shape was detected. Arrows indicate crest direction for ebb tide (in geographic degrees). Overlain in (**ii**) black line shows dune outline position and position of halo surrounding dune from June survey in (**i**).

However dune profile data from multi-beam survey data (Meygen LTD, 2009, [3]), which was undertaken on an ebb-tide indicate that subaqueous dunes on the northern edge slope to the east and the small dunes on the southern edge slope to the west, indicating a clockwise current direction around the dune when the multi-beam data were collected during ebb tide (Figure 5). The oval shape of this sediment bank and its position is related to a tidal eddy, which the side-scan and multibeam survey results suggest flows in a counter-clockwise rotation during flood tide and clockwise rotation during ebb tide.

The southern wedge shaped sediment bank is not mapped in its entirety, but multi-beam survey data show it to be a minimum of 2 km in length, being approximately 450 m in width at the eastern side of the Inner Sound [3]. This feature eventually forms a wider formation out-with the sound and study area to the east which has not yet been fully mapped.

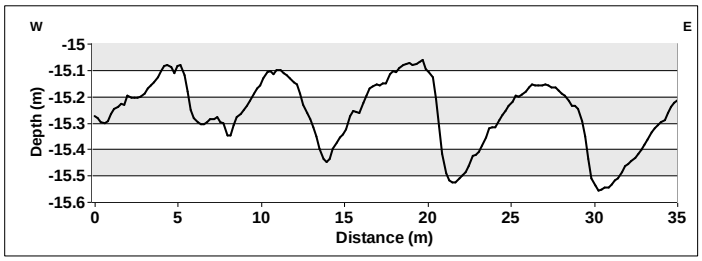

(**i**)

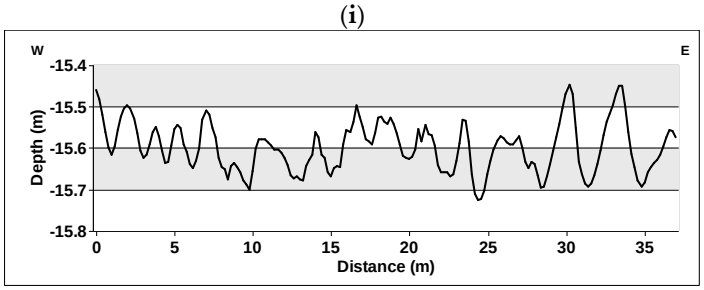

(**ii**)

Figure 5. *Cont.*

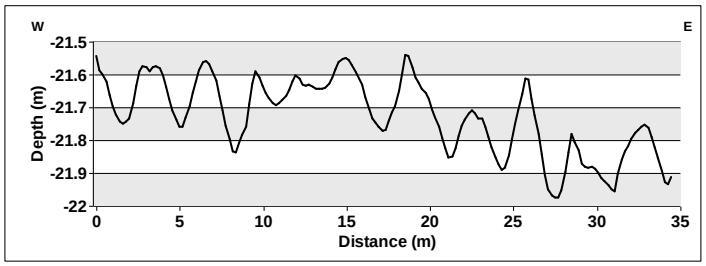

(iii)

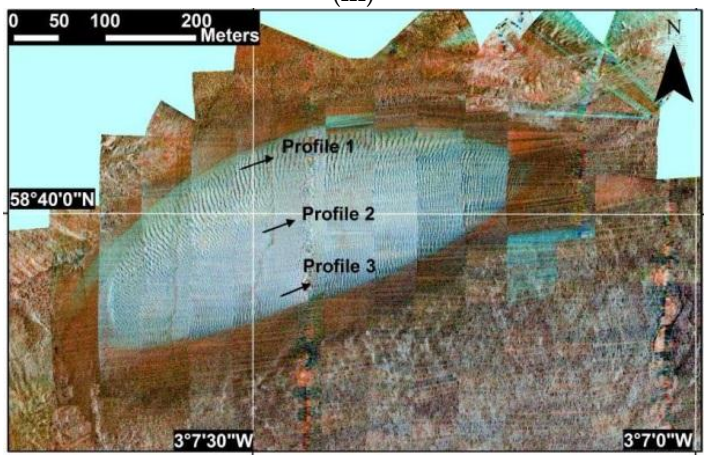

(iv)

Figure 5. (**iv**) Position of dune profiles along three sections on the oval dune overlain on survey 2 (June 2015); Profile bathymetric data from multi-beam data collected during the ebb phase (2009, 3(**i**) Profile 1 shows sand dunes with 40 cm amplitude and up to 7 m wavelength; (**ii**) Profile 2 showing small dunes in the centre of the oval dune, Amplitudes of ~10 cm and 1–2 m wavelength; (**iii**) Profile 3 showing smaller sand dunes on the southern edge of the oval sediment bank. Amplitudes of 20 cm and wavelength of 2–3 m

The largest dunes superimposed on the southern wedge shaped sediment bank are found on its northern edge with wavelengths varying between 10 and 30 m. On its southern side dunes have crests between 10 and 15 m. Smaller dunes exist in the centre of the formation with wavelengths of approximately 5 m.

The wedge shaped southern sediment bank shows a change in direction of the dune slope orientation with crests sloping toward approximately 250° N during survey 1 (ebb tide, June 2016) and toward 70° N during survey 2 (flood tide May 2016, Figure 6). No change was observed in the plan position of the wedge shaped bank in the two side-scan surveys undertaken. This is also the case when compared to a much earlier multi-beam survey obtained by Meygen LTD in September 2009 [3].

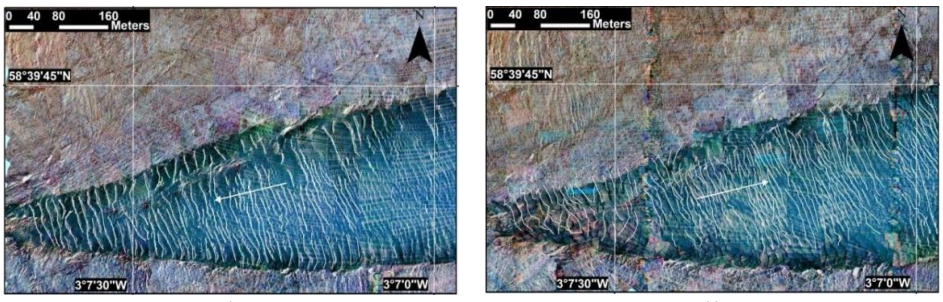

(i) (ii)

Figure 6. Side-scan mosaic showing shell bed dune orientation during spring ebb tide (**i**) and spring flood tide (**ii**).

Seabed profiles obtained from the multi-beam survey show similar dune wavelengths as the side-scan surveys (Figures 5 and 7). Figure 7 illustrates the wavelengths and amplitudes of the sand dunes on the northern edge of the wedge shaped sediment bank. The multi-beam survey shows little difference, with wavelengths on the surface of the sediment bank compared with the side-scan surveys presented here.

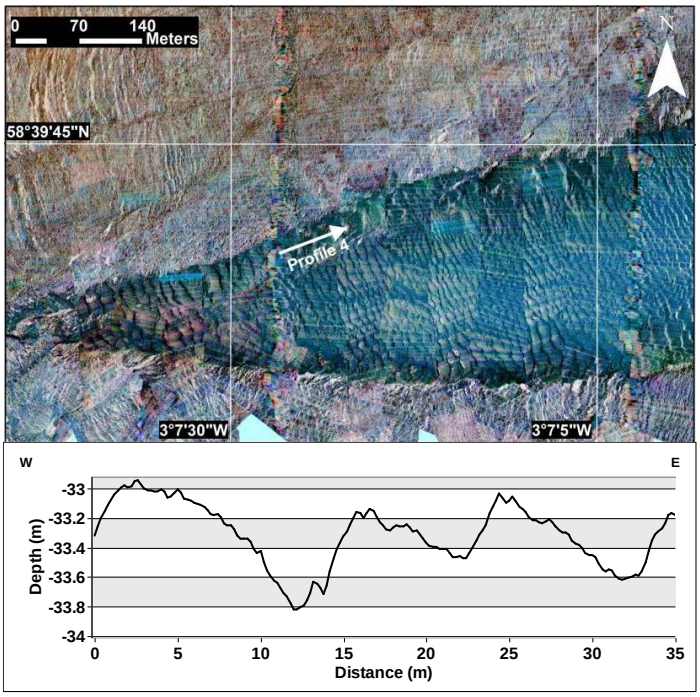

Figure 7. (**Top**) Profile from the multi-beam survey 2 (June 2016, ebb tide) taken on the wedge shaped sediment bank, arrow indicates start and stop of profile line; (**Bottom**) Profile 4 showing large sand dune formation on the northern edge of the wedge shaped sediment bank. Wavelengths of >10 m and amplitudes up to 1 m.

3.2. ROV and Sediment Grabs

Small sediment grab samples were taken and standard particle size analysis undertaken. Samples from the northern sediment bank were found to be unimodal, moderately well sorted medium grained sand, with a mean grain size (D50) of 354.18 µm taken from an average of five samples (Figure 8).

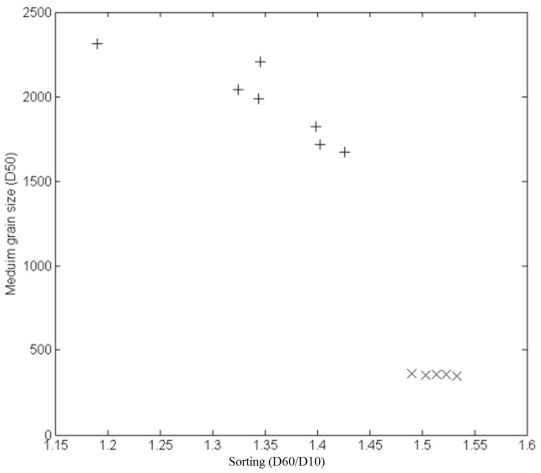

Figure 8. Grain size distributions for the shell fragments (+) and medium grain sand (×).

Sediment samples recovered from the wedge shaped sediment bank showed the material to be almost exclusively fragmented carbonate shell (0.1% medium sand present in average of all samples). There are other such examples of biogenic shell banks surrounding the Pentland Firth area and have been found to be composed almost exclusively of carbonate shell fragments [11–13]. Standard particle analysis is not well suited to this material due to the non-spherical nature of the shell fragments. However particle size analysis showed it to be very coarse sand to fine gravel texturally with a mean grain size of 1966 µm from an average of seven samples.

ROV still images show the sediment banks *in situ*; the green dots present on the image are laser points from the ROV indicating a scale of approximately 20 cm. ROV surveys revealed that the halo of material evident in side-scan sonar imagery surrounding the oval shaped sediment bank was composed of smoothed rounded rock cobbles. Cobbles were estimated to be between 4 and 6 cm in diameter on average with larger cobbles present (up to 15 cm diameter). Between the cobbles, shell fragments similar to those found in the southern wedge shaped bank were found (Figure 9). Kelp fronds are present in areas of the halo growing on the cobbles.

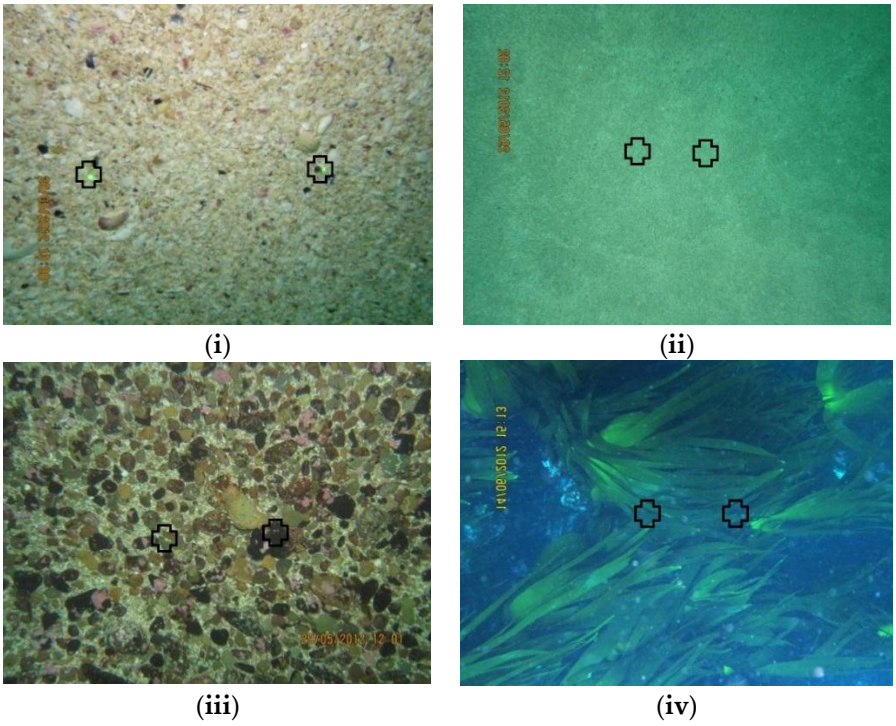

Figure 9. ROV images showing shell material from the wedge shaped sediment bank (**i**) and medium grained mineral sand from the oval shaped bank in the north of the study area (**ii**); Cobble halo surrounding oval shaped sediment bank to the north of the study area (**iii**) and kelp covered bedrock (**iv**). Markers show position of laser markers showing approximate 20 cm scale. (Laser markers only visible in high resolution image).

3.3. Acoustic Doppler Current Profiler (ADCP)

The ADCP survey revealed the area of fastest flow during flood tide lay within the southern central section of the channel, on the southern edge of the wedge shaped shell bank, with current speeds reaching almost 3 $m \cdot s^{-1}$ during this survey. Currents were much weaker in the northern part of the channel, but the ADCP survey did not extend into the bay on the southern coast of Stroma (Figure 9). The ebb tide currents were strongest at the western end of the channel, again reaching speeds of almost 3 $m \cdot s^{-1}$. In the central channel, ebb tide currents were much weaker than during flood tide, but this is mostly explained by the smaller tidal range at the time of the ebb tide survey.

The velocity profile in the vicinity of the shell bank in the central channel demonstrated that speeds were greater than 2 m·s^{-1} but less than 3.5 m·s^{-1}. The material in the shell banks is therefore resistant to relatively high flow speeds. Current speeds along the southern edge of the shell bank increase with velocities exceeding 3.5 m·s^{-1}. At peak spring tides, instantaneous flow speeds in the central channel 6 m s-1 have been recorded [15].

3.4. Hydrodynamic Modelling

The hydrodynamic model satisfactorily reproduced the tide at tide gauge locations around the northern Scotland coastline including both ends of the Pentland Firth (Table 1), a fundamental requirement since currents in the Firth are largely driven by sea level pressure gradients [15]. We varied the frictional drag coefficient, CD, over an order of magnitude from CD = 0.001 to CD = 0.01 and found best agreement with the data with mid-range values. The model results reported here are from the simulation with CD = 0.004. Modelled tidal height constituent amplitudes were typically within $\pm$0.04 m, and phases within 10°.

Figure 10 shows flood (i) and ebb (ii) underway ADCP measurements which show similarity to the modelled output (Figure 11).

Table 1. Modelled and observed amplitude (m) and phase (°) of the tidal height for the five principal tidal constituents at five locations around the Pentland Firth (see Figure 1).

Site		O_1		K_1		N_2		M_2		S_2	
Scrabster	Gauge	0.10	351	0.14	142	0.29	219	1.36	244	0.51	277
	Model	0.09	10	0.13	143	0.29	218	1.36	243	0.51	277
ADCP 2 (Acoustic Doppler Current Profiler)	Gauge	0.11	7	0.09	170	0.16	250	0.94	279	0.43	317
	Model	0.10	17	0.12	156	0.20	250	0.97	274	0.34	310
Stroma	Gauge	0.11	1	0.13	176	0.17	249	0.89	282	0.36	325
	Model	0.10	18	0.12	157	0.18	254	0.92	278	0.32	314
John O'Groats	Gauge	0.10	8	0.11	161	0.18	257	0.83	284	0.28	320
	Model	0.09	23	0.11	161	0.18	261	0.93	284	0.31	321
Wick	Gauge	0.11	29	0.10	176	0.18	298	0.96	322	0.32	1
	Model	0.09	34	0.11	173	0.19	291	0.97	312	0.33	351

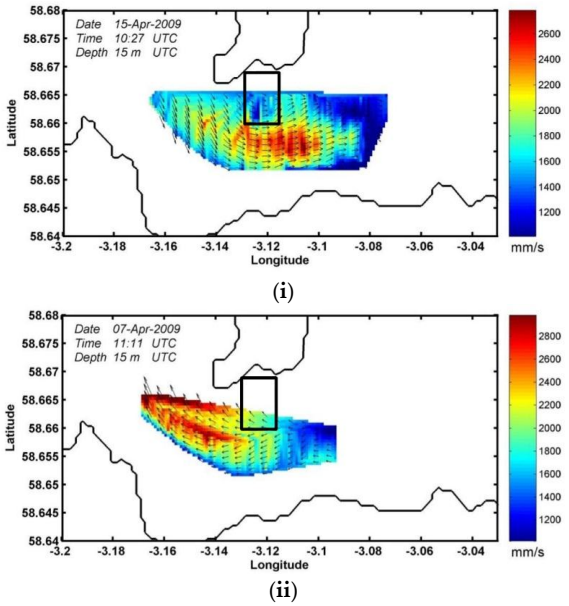

Figure 10. ADCP observations of tidal currents during flood (**i**) and ebb (**ii**) tides, from April 2009. The tidal currents were corrected for temporal distortion using a method described in [12], resulting in currents estimated at mid-track time. Study area marked with black rectangle.

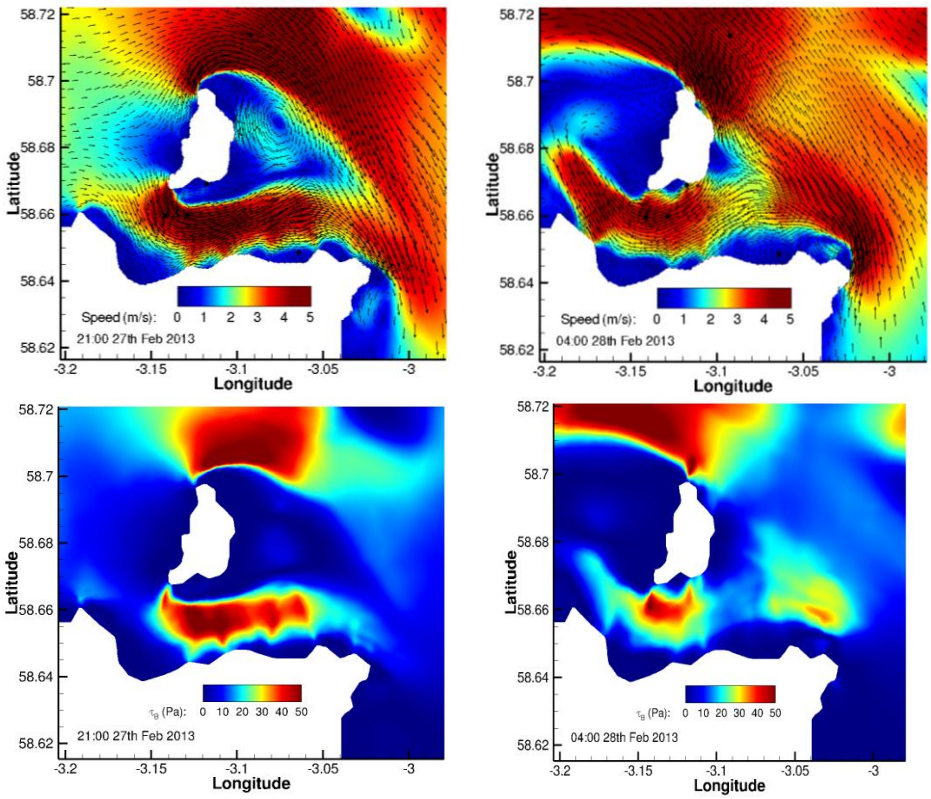

Figure 11. Model-predicted depth-averaged currents on a spring flood (**top left**) and spring ebb (**top right**) on 27–28 February 2013. Current vectors (m s^{-1}) are overlain on the coloured current speed (m s^{-1}). The bed shear stress (Pa) for the corresponding flood (**bottom left**) and ebb (**bottom right**) tides are calculated using Equation (1).

Comparison with moored ADCP data also showed similarity in the magnitudes and phases of velocity for the principal tidal constituents (Table 2). The M_2 tidal constituent dominated both the regional tides and particularly the tidal currents in the Inner Sound, being 2.5 times stronger than the next largest constituent S_2 (Table 2).

Table 2. Modelled and observed amplitude (m s^{-1}) and phase (°) of the tidal velocities for the principal tidal constituents.

Site		O_1		K_1		N_2		M_2		S_2	
ADCP 1	Obs	0.11	285	0.08	130	0.44	211	2.59	240	1.09	278
	Model	0.05	324	0.11	92	0.48	203	2.70	239	0.85	269
ADCP 2	Obs	0.09	281	0.07	111	0.48	202	2.92	239	1.17	274
	Model	0.05	322	0.11	93	0.52	203	2.82	238	0.91	269

Modelled velocity fields show flow separation occurring at the northern and southern headlands of Stroma on the flood tide (Figure 11), with counter-eddies forming to the east. A large eddy attached to the northern stream forms in the lee of Stroma, whereas a smaller counter-eddy is trapped in the bay on the south coast of Stroma where the oval shaped sand dune is located. The model snapshot clearly illustrates the blocking effect of Stroma directing the tidal stream through the Inner Sound channel, with the core flood tidal stream steered southward into the centre of the channel. The shell bank is located along the northern periphery of the strongest flood currents. During the ebb tide, the model shows the strongest flow occurs closer to Stroma and at the western end of the channel, with the currents south of Stroma being weaker than during the flood tide. At the location of the flood tide

eddy, the flow is now partly shadowed by the headland to the east, with weaker currents evident. At the start of the ebb tide, the large eddy east of Stroma is swept north-westwards into the main Pentland Firth channel.

Bed shear stress on flood and ebb tides were calculated using Equation (1). On flood tides, modelled bed stress values increased from about 0.5 Pa off the southern coast of Stroma to more than 50 Pa in the central channel (Figure 11). On the ebb tide, the area of low values was confined more closely to the Stroma coast, and values were not so high in the central channel south of Stroma, peaking to the south-west of the island. High values (>50 Pa) are evident to the north of the island on both flood and ebb tides.

4. Discussion

4.1. Hydrodynamics of the Inner Sound

Both the observations and the hydrodynamic modelling presented here illustrate the asymmetry in the tidal current regime through the Inner Sound. Flood tide currents entering the Sound from the west, are diverted southward into the centre of the channel by the headland at the south-western extremity of Stroma. The main flow is accelerated around the headland, forming a stream about 1 km wide through the channel wherein current speeds at spring tides regularly exceed 4.5 m s^{-1} (and have been recorded at up to 6 m$\cdot$ s^{-1}) to the south of Stroma. Previously published ADCP data 16 show similar features. Modelling results suggest a trapped counter-eddy develops in the bay on the south coast of Stroma, at the location where a persistent sand bank was observed. On the ebb tide, flows accelerate through the channel, with fastest speeds occurring to the south-west of Stroma. The ebb stream through the Inner Sound is shifted slightly north compared to the flood stream, since the headland at the south-east corner of Stroma does not protrude so far into the channel. In the central Inner Sound, current speeds during ebb tide are significantly less than during flood, and are orientated to the south-west rather than directly west. Maximum bed stress in the channel is therefore determined predominantly by the flood tide velocity field.

Predicted bed stress in the Sound during flood tide ranged from about 0.5 Pa beneath the trapped eddy in the bay on the south coast of Stroma to values exceeding 50 Pa in the central channel and higher (>60 Pa) off headlands and in the main Pentland Firth channel north of Stroma. With flood tide bed stress values less than 1 Pa, we might expect to find medium or coarse sand beneath the eddy [8]; the sonar observations reported here, confirming the presence of an oval-shaped bank of medium sand in that location, therefore provide corroborating evidence for the numerical model predictions and, conversely, help us understand the persistent nature of the sandbank. Model simulations reveal that the flood tide counter-eddy in the bay is a persistent feature and that the bank is also protected from the ebb tide currents by the headland to the east.

To the south of the eddy, bed stresses increase rapidly into the central channel. Bed stress values of up to 25 Pa might allow coarse gravel sediments to persist [8]. The wedge-shaped bank observed by the sonar certainly lies in an area where bed stress values can be relatively high; possible reasons for the presence of this bank are discussed in the following sections.

4.2. Grain Settling Velocity and Entrainment

A limitation of side-scan sonar with the frequencies used here (114–410 kHz), is that only the surface of the material is imaged. However after extensive ROV video surveys combined with sediment grabs, only shell fragments were observed to compose the wedge shaped southern bank. It is known that other such banks exist in the local region [11–13], an example of which is the Sandy Riddle, located approximately 13 km to the east composed almost exclusively of carbonate shell fragments [12]. Based on the ROV evidence, sample grab and surface sonar reflectivity of the bank it is expected the bulk composition of the southern wedge shaped bank is also carbonate shell fragments.

With this premise the composition and position of this bank can be attributed to the size, shape, and density of the shell fragments. Settling velocity, ω_s, can be calculated by differing empirical expressions in which the calculation of drag coefficient as a function of fluid and grain properties differs. Ferguson and Church [35], provide a simple expression which serves well for a variety of sediments:

$$\omega_s = \frac{RgD^2}{C_1 v + \left(0.75 C_2 RgD^3\right)^{\frac{1}{2}}} \quad (2)$$

where R is the submerged specific gravity, g is the acceleration due to gravity, v is the kinematic viscosity, D is the grain diameter in m, and C_1 is a constant with a theoretical value of 18 and represents the smoothness of the grains. C_2 is the constant asymptotic value of the drag coefficient. The drag coefficient is 1 for a spherical grain, natural mineralogical sediments have values ranging from 0.8 to 1.15 dependent on shape (Table 3).

Table 3. Smoothness and shape drag coefficient values for Equation (2).

Constant	Smooth Spheres	Natural Grains: Sieve Diameters	Natural Grains: Nominal Diameters
C_1	18	20	24
C_2	0.4	1	1.1

The important aspect to all such equations is the behaviour of a particle in a fluid in relation to the particles density and shape and most such equations are based on a near spherical particle such as natural mineralogical sand. Shell is not spherical or a near-spherical particle with near-spherical particles showing preferential transport in comparison [36]. Broken shell consists of a large diameter grain which is very thin in cross section [18]. This type of particle will have a larger drag coefficient when settling due to the large cross section area exposed to the upward force of the fluid, or a large lift surface [37]. The opposite is true once the shell material is settled, shell material generally settles on the side with the largest surface area, and the thin cross-section exposed to the current. In this configuration the drag coefficient is now much lower than natural sediment. Studies have suggested that drag coefficients for whole shells are a low as 0.09 or less [18]. A much lower drag coefficient requires a faster current to entrain the shell fragments, with bedforms having resistance to high flow when in a structured bed [37]. However the shape of shell particles makes it difficult to numerically predict the hydrodynamic response of the particles [18,19]. The initial movement of non-spherical grains is further complicated by turbulent flow. A standard method to quantitatively identify the inception of grain motion is the Shields parameter [38], however no universal method for all sediment types has yet been developed [39], with many researchers applying corrections with respect to specific sediment types [19,40].

No information is available on the deposition rate on either sediment bank, however similar shell banks within the geographical area have been estimated to have accumulation rates of 540 g/m^2 year. or 67 cm/1000 year. [11]. The shell material is provided by organisms growing on the local shelf which is thought to be of low diversity and abundance [12,13].

It is postulated that the southern wedge shaped sediment bank in the side-scan surveys can be viewed as a lag deposit composed primarily of carbonate shell fragments [20]. Mineral sand is present in very low quantities in all grab samples with carbonate shell fragments composing >99% of the sediment, it is likely mineral medium grained sand is swept through the channel or captured in the eddy formation and deposited on the medium grained sediment bank to the south of Stroma.

4.3. Inferred Sediment Dynamics

From available data a simple interpretation of the pattern of sediment within the Inner Sound can be speculated (Figure 12). The two sediment bodies present within the study area represent two

different hydraulic populations, in place due to the pattern of tidal currents, bathymetry, sediment availability, and sediment type. The difference in drag behaviour between natural sand and the shell fragments is an important factor in the observed sediment distribution.

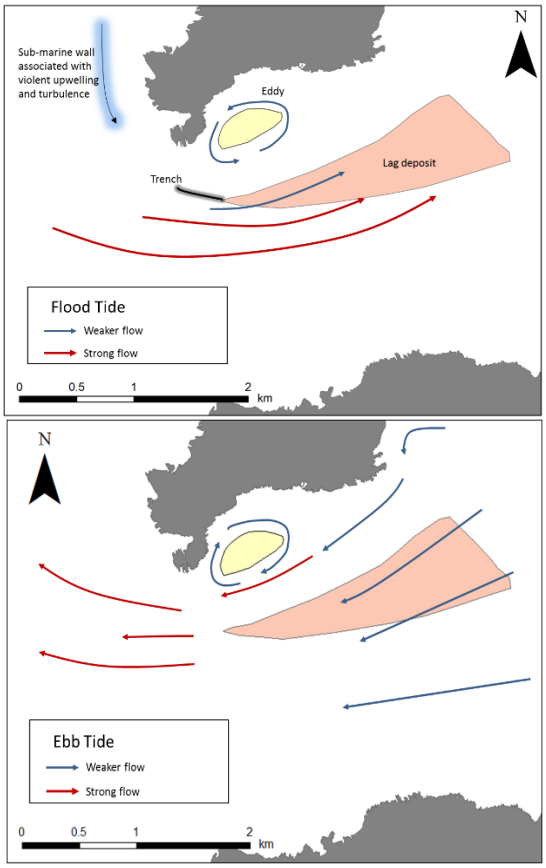

Figure 12. Inferred sediment dynamics during flood (**top**) and ebb (**bottom**) tides. The yellow oval bank is medium grained sand whilst the pink wedge shaped bank is carbonate shell.

Shell fragments can be seen in the water column visually and a possible local source for the shell to become entrained is near a submarine ledge which exists on the eastern side of Stroma. From ROV footage it is estimated that this feature is an almost vertical wall from approximately 15 m or more in depth to less than 5 m depth at spring low tide (chart datum). During flood tide this feature causes powerful turbulence with vortexes, explosive kolk-boil, which erupt on the surface running along the edge of the submarine ledge, this is a source of initial shell entrainment into the channel. Shell fragments are transported into the channel by bedload and suspended transport then deposited outside the main current flow during slack tide in reduced current speeds (Figure 12).

Finer grained natural mineral sediment is not able to settle until it is carried into a calm area and deposited on the centre of the eddy which exists to the east of the rocky prominence on the south side of the island. This sand bank is then shaped by the eddy feature during flood tide. During ebb tide the flow is not sufficient for entrainment of the shell fragments once settled with only surface remodelling occurring. Subaqueous dune direction change is evident between surveys taken during flood tide and ebb tide.

The shell fragments form a bedform which is resistant to high current flow although surface re-modelling occurs during different tidal phases. Tidal asymmetry is not sufficient to alter the plan position of the bank by bedload transport alone. From the inferred mechanics of deposition it is speculated that the sediment banks present in the inner sound are not transient features but have been locked in place by the pattern of current flow. The shell gravel bank and medium grained sand

bank may be sensitive to change in local hydrodynamics, in particular plan position of the shell bank. Settling velocities and entrainment velocities of the shell fragments are of importance when considering future sediment modelling of this region, in particular under turbulent flow.

4.4. Implications for Tidal Energy Extraction

The Inner Sound is the site of the likely first tidal turbine array to be deployed in the world [3], with installation commencing in 2016. Initially four turbines will be deployed, followed by, in a phased deployment programme, 82 more and eventually up to 279 turbines in total. Total energy generation is expected to reach up to 398 MW. Extracting energy from tidal systems is very likely to have effects on the sediment dynamics of the local area [6–9]. As the deployment of turbines in the Inner Sound proceeds, we can therefore expect to see changing patterns of sediment deposition and erosion in the Inner Sound, with evolving seabed sediment distributions. As described above, the currently observed sediment distributions are dependent on the prevailing hydrodynamics, and the shell bank in particular is sited in a narrow band of current conditions. An array of turbines to the south in the main tidal flow is likely to partially divert the flow around the array, due to partial blocking, and enhance the current speeds around the sides. It seems plausible, therefore that the shell bank may ultimately be eroded or, more likely, relocated by the changing hydrodynamics.

Monitoring the evolution of these sediment features following deployment of the turbines may be of scientific interest, in particular, by comparing numerical predictions with ongoing observations. This knowledge will be of value for regulators and the marine energy industry itself, in assessing potential impacts of proposed tidal arrays elsewhere in the UK and abroad. And whilst the sand and shell banks described here are small features, changes to the large scale sediment dynamics of the region may have knock-on effects on downstream benthic habitats [10], including marine protected areas, which often contain sessile filter feeding organisms dependent on suspended sediment transport for food. To understand the potential effects of wider marine energy development in the coastal zone over the coming years and decades, therefore requires fully calibrated and tested hydrodynamic and sediment transport models. Monitoring of sediment distributions in areas such as the Inner Sound will provide a valuable observational resource to test and develop those models.

5. Conclusions

The pattern and strength of tidal current flow within the Inner Sound has sorted the available sediment into two distinct sediment banks which have likely been locked in place for a significant time period and developed throughout the Holocene since sea level rise allowed.

Based on studies of similar sites in the region, deposition rates for both banks are expected to be low with sediment being reworked on the banks by tidal flow. The shape and density of the shell fragments affect drag; once deposited the bedform is highly resistant to high current velocities. Modelling of the transport of shell fragments will help in assessing the likely impact of change in hydrodynamics to the banks; however the difficulty remains in modelling the behaviour of irregularly shaped particles in turbulent flow.

Multi-frequency side-scan sonar and the introduction of colour to the processed imagery has improved classification of the seabed as compared with single frequency data.

Acknowledgments: Contribution to project TURNKEY (Transforming Underutilised Renewable Natural Resource into Key Energy Yields; project 2013-1/279) of the Atlantic Area Transnational Cooperation Programme financed by the European Regional Development Fund (ERDF). Thanks to Meygen Ltd. for supplying multi-beam data used in this paper, and to Jon Hardwick of the University of Exeter for providing us with the ADCP data from site ADCP 1 for model calibration. Sea level data from Wick were obtained from the British Oceanographic Data Centre. We are grateful to Roy Walters for providing his model code and his help in setting up the model of the Pentland Firth. We thank Konsberg Geoacoustics LTD for the loan of the tri-frequency sonar. We thank two anonymous reviewers for their suggestions which much improved the paper.

Author Contributions: Jason McIlvenny led the field work, undertook the data analysis and wrote the paper; Duncan Tamsett led the colour sonar development, wrote the GeoTexture software used to process the sonar

data, participated in the field work, processed the colour sonar data and co-wrote the paper; Philip Gillibrand undertook the tidal modelling work and co-wrote the paper; Lonneke Goddijn-Murphy undertook the underway ADCP survey, analysed the data and edited the manuscript.

Conflicts of Interest: The authors declare no conflict of interest.

References

1. Draper, S.; Adcock, T.A.A.; Borthwick, A.G.L.; Houlsby, G.T. Estimate of the tidal stream power resource of the Pentland Firth. *Renew. Energy* **2014**, *63*, 650–657. [CrossRef]
2. Adcock, T.A.A.; Draper, S.; Houlsby, G.T.; Borthwick, A.G.; Serhadlioglu, S. The available power from tidal stream turbines in the Pentland Firth. *Proc. R. Soc. A. Math. Phys. Eng. Sci.* **2013**, *469*, 1–21. [CrossRef]
3. Meygen Ltd. MeyGen Tidal Energy Project Phase 1 Environmental Statement. Available online: http://77.68.107.10/Renewables%20Licensing/MG_Sound_of_Stroma_Offshore_Tidal_Array/ES/Complete%20ES.pdf (accessed on 16 November 2015).
4. Shields, M.A.; Dillon, L.J.; Woolf, D.K.; Ford, A.T. Strategic priorities for assessing ecological impacts of marine renewable energy devices in the Pentland Firth (Scotland, UK). *Mar. Policy* **2011**, *33*, 635–642. [CrossRef]
5. Bonar, P.A.; Bryden, I.G.; Borthwick, A.G. Social and ecological impacts of marine energy development. *Renew. Sust. Energy Rev.* **2015**, *47*, 486–495. [CrossRef]
6. Neill, S.P.; Litt, E.J.; Couch, S.J.; Davies, A.G. The impact of tidal stream turbines on large-scale sediment dynamics. *Renew. Energy* **2009**, *34*, 2803–2812. [CrossRef]
7. Neill, S.P.; Jordan, J.R.; Couch, S.J. Impact of tidal energy converter (TEC) arrays on the dynamics of headland sand banks. *Renew. Energy* **2012**, *37*, 387–397. [CrossRef]
8. Martin-Short, R.; Hill, J.; Kramer, S.C.; Avdis, A.; Allison, P.A.; Piggott, M.D. Tidal resource extraction in the Pentland Firth, UK: Potential impacts on flow regime and sediment transport in the Inner Sound of Stroma. *Renew. Energy* **2015**, *76*, 596–607. [CrossRef]
9. Fairley, I.; Masters, I.; Karunarathna, H. The cumulative impact of tidal stream turbine arrays on sediment transport in the Pentland Firth. *Renew. Energy* **2015**, *80*, 755–769. [CrossRef]
10. Harendza, A. Benthic habitats in a tide-swept channel of the Pentland Firth and their potential responses to a tidal energy development. Ph.D. Thesis, University of Aberdeen, Aberdeen, UK, 2014.
11. Farrow, G.E.; Allen, N.H.; Akapan, E.B. Bioclastic carbonate sedimentation on a high-latitude, tide-dominated shelf. NE Orkney Islands, Scotland. *J. Sed. Petrol.* **1984**, *54*, 373–393. [CrossRef]
12. Kenyon, N.H.; Cooper, W.S. Sand banks, sand transport and offshore wind farms. *DTI Strategic Environmental Assessment Area 6, Irish Sea, Seabed and Surficial Geology and Processes*; Report CR/05/057; British Geological Survey: Nottingham, UK, 2004. Available online: https://www.gov.uk/government/publications/strategic-environmental-assessment-6-environmental-report (accessed on 5 April 2016).
13. Light, J.M.; Wilson, J.B. Cool-water carbonate deposition on the West Shetland shelf: A modern distally steepened ramp. In *Carbonate Ramps*; Wright, V.P., Burchette, T.P., Eds.; Geological Society Special Publications: London, UK, 1998; Volume 149, pp. 73–105.
14. Holmes, R.; Bulat, J.; Henni, P.; Holt, J.; James, C.; Kenyon, N.; Leslie, A.; Long, D.; Musson, R.; Pearson, S.; *et al. DTI Strategic Environmental Assessment Area 5 (SEA5): Seabed and Superficial Geology and Processes*; British Geological Survey Report CR/04/064N; British Geological Survey: Nottingham, UK, 2005.
15. Easton, M.C.; Woolf, D.K.; Bowyer, P.A. The dynamics of an energetic tidal channel, the Pentland Firth, Scotland. *Cont. Shelf Res.* **2013**, *48*, 50–60. [CrossRef]
16. Goddijn-Murphy, L.; Woolf, D.K.; Easton, M.C. Current Patterns in the Inner Sound (Pentland Firth) from Underway ADCP Data. *J. Atmos. Oceanic Technol.* **2013**, *30*, 96–111. [CrossRef]
17. Tamsett, D.; McIlvenny, J.; Watts, A. Colour sonar: Multi-frequency side-scan sonar images of the seabed in the Inner Sound of the Pentland Firth, Scotland. *J. Mar. Sci. Eng.* **2016**, *4*, 1–18. [CrossRef]
18. Ramsdell, R.C.; Miedema, S.A.; Talmon, A.M. Hydraulic transport of sand/shell mixtures. In Proceedings of the ASME 2011 30th International Conference on Ocean, Offshore and Arctic Engineering OMAE 2011, Rotterdam, The Netherlands, June 19–24 2011.
19. Paphitis, D.; Collins, M.B.; Nash, A.I.; Wallbridge, S. Settling velocities and entrainment thresholds of biogenic sands (shell fragments) under unidirectional flow. *Sedimentology* **2002**, *49*, 211–225. [CrossRef]

20. Flemming, B.W.; Schubert, H.; Hertweck, G.; Muller, K. Bioclastic tidal channel lag deposits: A genetic model. *Senckenberg. Marit.* **1992**, *22*, 109–129.
21. Ashley, G.M. Classification of large-scale subaqueous bedforms: A new look at an old problem. *J. Sediment. Petrol.* **1990**, *60*, 160–172.
22. Folk, R.L.; Ward, W.C. Brazos River bar: A study in the significance of grain size parameters. *J. Sediment. Petrol.* **1957**, *27*, 3–26. [CrossRef]
23. Tamsett, D.; Hogarth, P. Side-scan sonar beam function and seabed backscatter functions from trace amplitude and vehicle roll data. *IEEE J. Ocean. Eng.* **2015**, *41*, 155–163. [CrossRef]
24. Pawlowicz, R.; Beardsley, B.; Lentz, S. Classical tidal harmonic analysis including error estimates in MATLAB using T_TIDE. *Comput. Geosci.* **2002**, *28*, 929–937. [CrossRef]
25. Walters, R.A.; Casulli, V. A robust, finite element model for hydrostatic surface water flows. *Comm. Numer. Methods Eng.* **1998**, *14*, 931–940. [CrossRef]
26. Walters, R.A. Coastal ocean models: Two useful finite element methods. *Cont. Shelf Res.* **2005**, *25*, 775–793. [CrossRef]
27. Walters, R.A. A semi-implicit finite element model for non-hydrostatic (dispersive) surface waves. *Int. J. Numer. Methods Fluids* **2005**, *49*, 721–737. [CrossRef]
28. Gillibrand, P.A.; Lane, E.M.; Walters, R.A.; Gorman, R.M. Forecasting extreme sea surface height and coastal inundation from tides, surge and wave setup. *Aust. J. Civil Eng.* **2011**, *9*, 99–112.
29. Lane, E.M.; Gillibrand, P.A.; Arnold, J.R.; Walters, R.A. Tsunami inundation modeling with RiCOM. *Aust. J. Civil Eng.* **2011**, *9*, 83–98.
30. Walters, R.A.; Gillibrand, P.A.; Bell, R.; Lane, E.M. A Study of Tides and Currents in Cook Strait, New Zealand. *Ocean Dyn.* **2010**, *60*, 1559–1580. [CrossRef]
31. Plew, D.R.; Stevens, C.L. Numerical modelling of the effect of turbines on currents in a tidal channel–Tory Channel, New Zealand. *Renew. Energy* **2013**, *57*, 269–282. [CrossRef]
32. Walters, R.A.; Tarbotton, M.R.; Hiles, C.E. Estimation of tidal power potential. *Renew. Energy* **2013**, *51*, 255–262. [CrossRef]
33. Egbert, G.D.; Erofeeva, S.Y. Efficient inverse modelling of barotropic ocean tides. *J. Atmos. Ocean. Technol.* **2002**, *19*, 183–204. [CrossRef]
34. Dyke, P.P.G. *Coastal and Shelf Sea Modelling*; Springer US: New York, NY, USA, 2001.
35. Ferguson, R.I.; Church, M. A simple universal equation for grain settling velocity. *J. Sediment. Res.* **2004**, *74*, 933–937. [CrossRef]
36. Durafour, M.; Jarano, A.; Le Bot, S.; Blanpain, O.; Lafite, R.; Marin, F. *In-situ* study of the influence of size and shape of sediments on bedload transport. In Proceedings of the 7th International Conference on Coastal Dynamics, Bordeaux, France, 24–28 June 2011; pp. 541–552.
37. Weill, P.; Mouazé, D.; Tessier, B.; Brun-Cottan, J. Hydrodynamic behaviour of coarse bioclastic sand from shelly cheniers. *Earth Surf. Process. Landf.* **2010**, *35*, 1642–1654. [CrossRef]
38. Shields, A. Anwendung der Aehnlichkeitsmechanik und der Turbulenzforschung auf die Geschiebebewegung [Application of similarity mechanics and turbulence research on shear flow]. *Mitt. Preußischen Vers. Wasserbau* **1936**, *26*, 5–24.
39. Valyrakis, M.; Diplas, P.; Dancey, C.L. Entrainment of coarse grains in turbulent flows: An extreme value theory approach. *Water Resour. Res.* **2011**, *47*, 1–17. [CrossRef]
40. Smith, D.A.; Cheung, K.F. Transport rate of calcareous sand in unidirectional flow. *Sedimentology* **2005**, *52*, 1009–1020. [CrossRef]